Velocity Map Imaging Spectroscopy of C_2H^- and C_2D^-: a benchmark study of vibronic coupling interactions

Benjamin A. Laws,[*,†,‡] Zachariah D. Levey,[†] Andrei M. Sanov,[¶] John F. Stanton,[§] Timothy W. Schmidt,[†] and Stephen T. Gibson[‡]

†*School of Chemistry, University of New South Wales, Sydney NSW 2052, Australia*

‡*Research School of Physics, The Australian National University, Canberra ACT 2601, Australia*

¶*Department of Chemistry and Biochemistry, The University of Arizona, Tucson, Arizona 85721, United States*

§*Department of Chemistry, University of Florida, Gainesville, Florida 32611, United States*

E-mail: b.laws@unsw.edu.au

Abstract

High-resolution velocity map imaged photoelectron spectra of the ethynyl anions C_2H^- and C_2D^- are measured over a range of photodetachment wavelengths, to investigate the complex interactions between the close lying $\tilde{X}^2\Sigma^+$ and $\tilde{A}^2\Pi$ electronic states. Vibronic coupling calculations are performed by transforming to a quasidiabatic representation, parametrised by *ab-initio* CFOUR calculations, to model the interplay between psuedo Jahn-Teller and Renner-Teller coupling. This approach is combined with electron anisotropy measurements to assign all of the observed vibronic structure, providing a framework that may be used to accurately simulate spectra of larger $C_{2n}H$ monohydride carbon chains.

Introduction

Carbon monohydrides $C_{2n}H$, are a class of linear radicals that play an important role in combustion and interstellar chemistry.[1–4] These carbon chains have been observed in many interstellar environments, including planetary atmospheres,[4–6] comets,[7] dark clouds,[8,9] and during heavy star formation.[10,11] Due to their relatively high abundance in a variety of astronomical conditions, they are believed to be promising candidates for Diffuse Interstellar Band (DIB) carriers.[9,12–16] The corresponding anions $C_{2n}H^-$ are also believed to play an important role in interstellar chemistry.[9,17] C_6H^- was the first negative ion detected in space, after it was observed in two distinct interstellar molecular clouds IRC+10216 and TMC-1 in 2006.[18] More recently, anions C_4H^- [19] and C_8H^- [20,21] have also been detected in a range of environments, include dark clouds,[22] prestellar cores,[23] and prostellar envelopes.[24]

Chain growth of the $C_{2n}H$ radicals occurs predominately through acetylene addition,

$$C_{2n}H + C_2H_2 \rightarrow C_{2n+2}H + H_2. \quad (1)$$

Conversely, the formation of anions in space is believed to be driven by radiative electron

attachment, charge transfer, and dissociate electron attachment. Current astrochemical modelling of interstellar clouds, such as IRC+1026, typically underestimate the observed abundances of CH_4^-.[17,22,25] Therefore, it has been proposed that ion-neutral reactions

$$C_{2n}H^- + C_2H_2 \rightarrow C_{2n+2}H^- + H_2. \tag{2}$$

may be significant chain growth mechanisms that also needs to be included in astrochemical models.[17,26] Studies of the extraterrestrial planetary atmosphere of Saturn's moon Titan, suggest that both C_2H and C_2H^- play an important role in the atmospheric chemistry.[6,27–29] Multiple reaction pathways involving the C_2H^- have been proposed, including reactions with C_2H_2 and HCN.

Our knowledge of interstellar chemistry relies critically on theory, to provide a link between astronomical observations and terrestrial laboratory studies. Microwave spectroscopy has successfully been used in this fashion to identify a large number of molecules in the interstellar medium (ISM). However for some species, particularly those with low abundances or no dipole moment, UV/vis spectroscopic methods are required for identification.[30] This creates a challenge for theory, as electronic spectra calculations are more sensitive to the level of theory employed than pure rotational spectra.[31] This becomes even more challenging when vibronic coupling effects are introduced, as they can be exceedingly difficult to model.

These considerations may be explored by examining some of the smallest carbon monohydrides. The ethynyl radical C_2H may appear to be a simple linear triatomic molecule. However the electronic spectrum is complicated by the presence of the close-lying ground $^2\Sigma^+$ and first excited $^2\Pi$ surfaces, which are only separated by $\sim 3,700$ cm^{-1}.[32,33] The interaction of these surfaces produces a complex vibronic spectrum around the $\tilde{A}^2\Pi$ state, where the $\tilde{X} - \tilde{A}$ origin is spread over multiple admixed vibronic levels. In C_4H the $^2\Sigma^+$ and $^2\Pi$ states are nearly degenerate, resulting in even stronger coupling,[34] while in C_6H and C_8H the ordering of the states swaps, with a ground $^2\Pi$ state and a low lying excited $^2\Sigma^+$

state.[35,36] Consequently, understanding these vibronic coupling interactions between the $^2\Sigma$ and $^2\Pi$ surfaces will be essential in order to accurately model the role these radicals (and their corresponding anions) are likely to play in the interstellar chemistry mentioned above, and to guide the search for possible DIB carriers.

In this work the vibronic spectrum of the ethynyl radical C_2H is examined by employing High-Resolution Photoelectron Imaging (HR-PEI) in order to benchmark CFOUR[37] *ab-initio* vibronic-coupling calculations. C_2H is reported to be one of the most abundant molecules in the universe, and is the most thoroughly studied of the $C_{2n}H$ species.[3,31,38] Many different experimental techniques have been employed to try and resolve the complex vibronic spectrum, including electron spin resonance,[39,40] laser magnetic resonance,[41–43] microwave and milli-meter wave spectroscopy,[44–47] infrared (matrix isolation[48–50] and Fourier Transform emission[51]) spectroscopy, laser induced fluorescence spectroscopy[52–54] and photoelectron spectroscopy.[34,36,55] C_2H has also received extensive theoretical attention to try and understand the experimental results, however the large number of possible vibronic levels means this has proven to be a challenge.[31,33,56–64] In this work we demonstrate how the construction of a quasidiabatic Hamiltonian allows for the strength of vibronic interactions between coupled surfaces near a conical intersection to be calculated, in order to simulate electronic and vibronic spectra. By employing anion HR-PEI both the $^2\Sigma^+$ and $^2\Pi$ surfaces are mapped out on an equal footing from the anion $\tilde{X}^1\Sigma^+$ state, allowing a direct comparison with *ab-initio* modelling.

Results and Analysis

Ethynyl ions were produced in a pulsed-jet discharge of pure C_2H_4 gas, and subsequently mass isolated via time of flight. Electrons were detached using a tuneable Continuum Sunlite Ex Optical Parametric Oscillator (OPO) pumped with the third harmonic of a Nd:YAG laser. High electron counts could also be obtained by using the third and fourth harmonics of the

Nd:YAG laser directly. Detached electrons are mapped onto a micro channel plate detector using a Velocity Map Imaging (VMI) lens. An illustrative VMI of ∼4 million electrons collected from 355 nm (3.49 eV) photodetachment of C_2H^- is shown in Fig. 1(a). The electrons are distributed radially according to their speed, with slow electrons at the image center, and fast electrons located towards the outer edge. Due to the relatively large C_2H electron affinity (EA) of 2.969 eV,[55] photodetachment at 355 nm occurs close to threshold. This yields slow electrons, allowing for a low repeller voltage (−600 V) on the VMI lens, and high velocity resolution.

Despite being close to threshold, two electronic states of neutral C_2H are observed. The faster electrons on the outer edge correspond to $C_2H(\tilde{X}\,^2\Sigma^+) + e^- \leftarrow C_2H^-(\tilde{X}\,^1\Sigma^+) + h\nu$ photodetachment, and are preferentially distributed around the poles of the image, indicative of a positive anisotropy parameter. Conversely the angular distribution of the slower electrons near the center are skewed towards the equator, indicative of a negative anisotropy parameter. These electrons may be assigned to photodetachment to the first excited state $C_2H(\tilde{A}\,^2\Pi) + e^- \leftarrow C_2H^-(\tilde{X}\,^1\Sigma^+) + h\nu$.

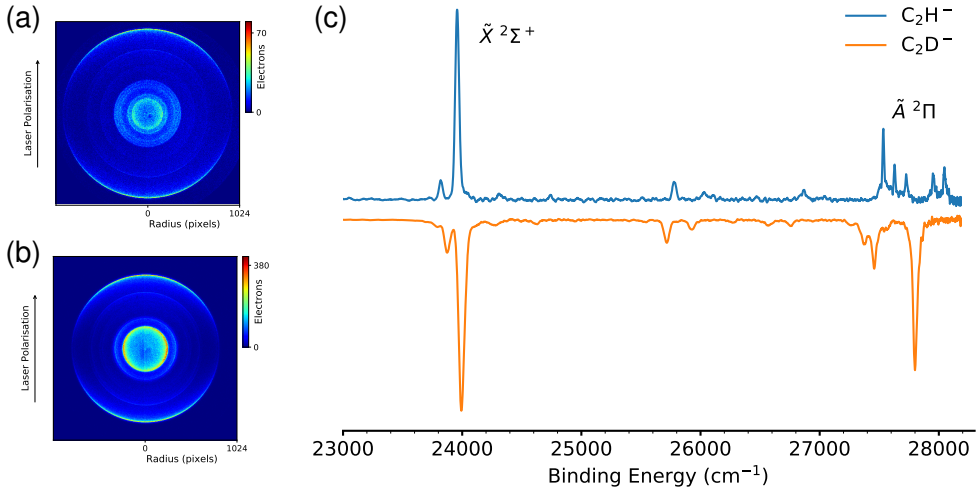

Figure 1: (a) Velocity map image of C_2H^- photodetachment at 355 nm. (b) Velocity map image of C_2D^- at 355 nm. (c) Comparison of 355 nm photoelectron spectra from C_2H^- and C_2D^-. Structure below $\sim 27,000$ cm^{-1} is assigned to the ground state $\tilde{X}^2\Sigma^+$, and structure above $\sim 27,000$ cm^{-1} is assigned to the excited $\tilde{A}^2\Pi$ state.

To investigate the vibronic coupling interaction between these two nearby Σ^+ and Π surfaces, deuterated ethynyl C_2D^- was also studied. C_2D^- ions were produced in a discharge of pure C_2D_4 gas and measured under the same experimental conditions as C_2H^-. An illustrative VMI of photodetachment at 355 nm from C_2D^- is shown in Fig. 1(b). Similarly to Fig 1(a) two electronic transitions are observed. While the fast electrons appear similar in both images, a striking difference is observed in the slow electrons near the detector center. In Fig. 1(a) a series of weak rings are observed, however in Fig. 1(b) the image is dominated by two distinct rings.

The VMIs in Fig. 1 were inverted using the Abel inversion methods detailed in PyAbel,[65] to extract the corresponding photoelectron spectra presented in Fig. 1(c). Below $27,000$ cm^{-1} on the $\tilde{X}^2\Sigma^+$ surface the C_2H^- and C_2D^- spectra are a close match. Both are dominated by the origin transition, shifted by ~ 10 cm^{-1} in the deuterated spectrum, with progressions involving the $\nu_2(\pi)$ bending and $\nu_3(\sigma)$ CC stretch vibrational normal modes. This includes transitions involving an odd quanta of ν_2 bending excitation (2^{n+1}) which should be totally forbidden within the harmonic oscillator approximation. However, the presence of these transitions in the spectra is likely an indicator of Herzberg-Teller (HT) vibronic coupling between the ground $^2\Sigma^+$ and nearby excited $^2\Pi$ electronic surfaces, as,

$$\Sigma^+ \otimes \pi = \Pi. \tag{3}$$

Above $27,000$ cm^{-1}, near the $\tilde{A}^2\Pi$ state origin, significant differences are observed between the C_2H^- and C_2D^- photoelectron spectra. In the C_2H^- spectrum 5 sharp peaks are observed, spaced by ~ 95 cm^{-1}. However in the deuterated spectrum, one dominant peak is observed at $27,792$ cm^{-1}, with 3 weaker peaks centred around $27,360$ cm^{-1}. Unlike the structure below $27,000$ cm^{-1} none of these peaks are able to be readily assigned to vibronic transitions, due to the presence of strong coupling interactions between the nearby Σ^+ and Π surfaces.

Vibronic Coupling Interactions

The complex spectral structure observed near the $\tilde{A}^2\Pi$ state origin in Fig. 1(c) may be understood by considering the v_2 bending vibrational mode. To account for the degeneracy of this mode, the vibronic quantum number ℓ_i may be introduced, representing the angular momentum associated with the bending motion. This may take a value of $\ell_i = v_i, v_i - 2, v_i - 4, \ldots, 1$ or 0, where v_i is the quanta of bending excitation. In the Born-Oppenheimer approximation different vibronic energy levels ℓ_i are degenerate, however in cases with strong rovibronic coupling, this degeneracy in ℓ_i is lost.

In C_2H this effect creates a Renner-Teller (RT) pair in the excited state, where the usually degenerate Π surfaces separate to form two non-degenerate electronic states $\Pi^+(2A')$ and $\Pi^-(1A'')$. This involves separating a single potential energy surface (V) into two distinct but coupled surfaces (V^+) and (V^-). Due to the strong coupling along the linear axis between the electronic and vibration angular momenta of the $2A'$ and $1A''$ components of the $^2\Pi$ state, stationary states cannot be explicitly assigned to either of the $\Pi^+(2A')$ or $\Pi^-(1A'')$ electronic surfaces. Instead, they exist as a combination of both states.

Due to the close lying nature of the ground $\tilde{X}^2\Sigma^+$ and excited $\tilde{A}^2\Pi$ electronic states, which are only separated by ~ 3700 cm^{-1}, a pseudo Jahn-Teller effect is also observed. In the case of C_2H this is seen as coupling between the ground $\Sigma^+(1A')$ and excited $\Pi^+(2A')$ states, induced by the bending motion of v_2. The ground state only couples to one of the Renner-Teller pair $\Pi^+(2A')$, as the other state $\Pi^-(1A'')$ has incorrect symmetry. This results in the complex vibronic structure observed for the $\tilde{A}^2\Pi$ electronic state, with contributions from three coupled surfaces $\Sigma^+(1A')$, $\Pi^+(2A')$, and $\Pi^-(1A'')$.

These interactions spread the electronic orgin of the $\tilde{A}\,^2\Pi$ state over several vibronic levels. Therefore, instead of assigning a defined origin, the observed peaks in the spectrum may be assigned to coupled admixtures of vibronic transitions involving the three potential

energy surfaces,

$$\Psi_f = \sum_{\xi} \psi_e^{\xi} \sum_k C_{fk}^{\xi} \phi_{fkm}^{\xi}, \tag{4}$$

where ψ_e^{ξ} is the diabatic electronic wavefunction, and ϕ_{fkm}^{ξ} is the spin-rovibrational wavefunction. ξ represents the electronic states used in the expansion ($\xi = \Sigma^+(1A')$, $\Pi^+(2A')$, $\Pi^-(1A'')$). Ref 33. A depiction of these three interacting surfaces is given in Fig. 2.

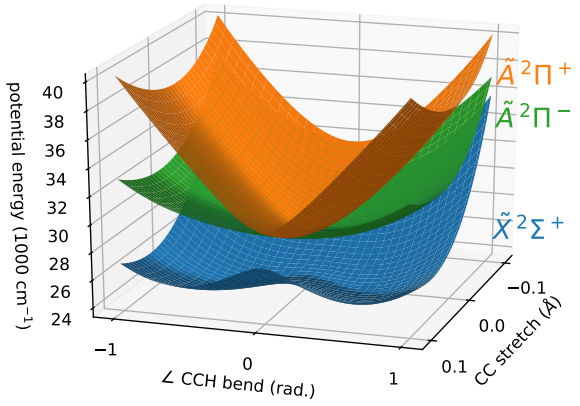

Figure 2: Adiabatic potential energy surfaces of $\tilde{X}^2\Sigma^+$, $\tilde{A}^2\Pi^-$, and $\tilde{A}^2\Pi^+$ states, calculated using the parameters calculated by Tarroni and Carter[33] ($E_{1A'}$, $E_{2A'}$, and $E_{1A''}$ in Eq. 4).

The adiabatic potential energy surfaces in Figure 2 were evaluated from the variational parameters of Tarroni and Carter.[61] Their technique calculates a multitude of admixed vibronic levels. In the literature, over 100 possible C_2H vibronic states have been calculated, up to 10,000 cm^{-1} above the $\tilde{X}^2\Sigma^+$ origin. However, assigning experimental spectra has remained a challenge, partly due to the large number of calculated levels providing multiple possible assignments for each experimentally observed transition.

Coupling Calculations

In order to guide spectral assignment of C_2H and astronomical searches for other C_nH radicals, transition intensities are also needed. However, due to the strong vibronic coupling interactions, this can not be obtained via standard quantum chemistry methods. To account

for these interactions, the photoelectron spectrum of the C_2H^- anion was simulated using a quasidiabatic Hamiltonian of the type advocated by Koeppel, Domcke and Cederbaum (KDC).[66,67] In this approach, the Hamiltonian is represented in a basis of quasidiabatic (slowly varying) electronic states for which the kinetic energy operator can be assumed diagonal.[68] For C_2H, the KDC Hamiltonian comprises three states - the two components of the $^2\Pi$ state and the ground $^2\Sigma^+$ state - and is then projected onto a vibrational basis, usually chosen as a direct product of harmonic oscillators. Diagonalization of the corresponding matrix yields the molecular states (which are given in terms of a Born-Huang expansion), and the squared projections of the corresponding eigenvectors onto the ground state of the anion yield the relative intensities. The latter is automatically true if the photodetachment cross sections for the $^2\Sigma^+$ and $^2\Pi$ states are assumed equal, but different cross sections of the two states can be incorporated by scaling the intensities of states according to their (vibronic) symmetry.[69]

Details of the construction and parametrization of KDC Hamiltonians can be found elsewhere in the literature,[63,70–73] and the procedure followed will be discussed here only briefly. The present calculations use the so-called quadratic vibronic coupling (QVC) model.[70] For the system at hand, the QVC model Hamiltonian assumes the following form

$$H = T_n 1 + V, \tag{5}$$

$$V = \begin{array}{c} \\ X \\ A(a') \\ A(a'') \end{array} \begin{array}{c} \begin{array}{ccc} X & A(a') & A(a'') \end{array} \\ \begin{pmatrix} \Delta_0^X + F_1^X q_1 + F_3^X q_3 + \frac{1}{2}\sum_{ij} F_{ij}^X q_i q_j & \lambda q_{2a} & \lambda q_{2b} \\ \lambda q_{2a} & \Delta_0^A + F_1^A q_1 + F_3^A q_3 + \frac{1}{2}\sum_{ij} F_{ij}^A q_i q_j + \frac{1}{2}\eta(q_{2a}^2 - q_{2b}^2) & \eta q_{2a} q_{2b} \\ \lambda q_{2b} & \eta q_{2a} q_{2b} & \Delta_0^A + F_1^A q_1 + F_3^A q_3 + \frac{1}{2}\sum_{ij} F_{ij}^A q_i q_j - \frac{1}{2}\eta(q_{2a}^2 - q_{2b}^2) \end{pmatrix} \end{array} \tag{6}$$

where the summations run over the dimensionless normal modes (q_i) that serve as the

coordinate system for the problem.[61,63] For convenience, the latter are chosen to be those of the anion, which considerably facilitates calculation of the spectral intensities. In Eq. (6), the diagonal terms of V (excluding those that carry the Renner-Teller coupling constant η) represent the quasidiabatic potential energy surfaces of the $^2\Sigma^+$, and the two components of the $^2\Pi$ state, chosen here as those in which the unpaired electron lies within or is perpendicular to an arbitrarily chosen plane, designated as A(a′) and A(a″), respectively. Δ_0^X is the separation of the anion and $^2\Sigma^+$ states at the origin of the coordinate system (the vertical electron detachment energy), and Δ_0^A is the gap between anion and $^2\Pi$ states at the same geometry.

For the modes of σ symmetry (q_1 and q_3), the diabatic forces (F_i) and force constants (F_{ij}) coincide with those of the adiabatic potential energy surfaces. However, for the bending mode, the diabatic (F_{22}) and adiabatic (f_{22}) force constants differ, and the parametrization is somewhat more involved. For each component of the $^2\Pi$ state, either the 2a or 2b component of the bending vibration will maintain the A′ electronic symmetry that is needed to couple with the $^2\Sigma^+$ state. Designating these as 2a for the A(a′) state and 2b for the A(a″) state (as is implicit in Eq. 6), the diabatic force constants for the bending mode in the $^2\Sigma^+$ and $^2\Pi$ states can be written as

$$F_{22}^X = f_{22}^X + \frac{2\lambda^2}{(\Delta_0^A - \Delta_0^X)} \tag{7}$$

$$F_{22}^A = f_{2a2a}^{A(a')} - \frac{2\lambda^2}{(\Delta_0^A - \Delta_0^X)} - \eta \tag{8}$$

where the Renner-Teller interaction strength (η) is determined from

$$\eta = \frac{1}{2}\left[f_{2a2a}^{A(a')} - f_{2b2b}^{A(a')} - \frac{2\lambda^2}{(\Delta_0^A - \Delta_0^X)}\right] \tag{9}$$

once the interstate coupling (λ which is calculated analytically in this work, see below) is known.

When the potential in Eq. (6) is diagonalized, the adiabatic states that are used for its parametrization are precisely recovered through terms second order in displacement. The linear diabatic coupling constants between the electronic states of interest were calculated analytically at the EOM-CCSDT/AN02 level of theory, using the CFOUR computational package[37] and the quasidiabatic ansatz of Ichino *et al.*[72] Briefly, the EOM procedure is used to operationally define quasidiabatic states (those that relax according to a well-behaved reference state wavefunction) and the coupling constants are then evaluated as the first derivative of the off-diagonal elements of the electronic Hamiltonian in the basis defined by this representation. The diabatic force and coupling constants calculated to parametrize the KDC potential in Eq. (6) are presented in Table 1.

Table 1: Parameters for the quasidiabatic Hamiltonian Eq. (6) determined using CFOUR and the quasidiabatic ansatz.

(I don't understand why these values are the same as C2H, when a 10cm-1 shift is observed in the spectrum)

	C_2H				C_2D			
	Anion	$\tilde{X}^2\Sigma^+$	$\tilde{A}^2\Pi(a')$	$\tilde{A}^2\Pi(a'')$	Anion	$\tilde{X}^2\Sigma^+$	$\tilde{A}^2\Pi(a')$	$\tilde{A}^2\Pi(a'')$
ΔE	0	22431.21	26543.67	26543.67	0	22431.21	26543.67	26543.67
f1	0	-211.28	286.9	286.9	0	-596.04	641.6	641.6
f2	0	-1515.21	1257.07	1257.07	0	-1401.53	1115.17	1115.17
f3	0	0	0	0	0	0	0	0
f4	0	0	0	0	0	0	0	0
f11	3424.32	3487.03	3482.16	3482.16	2611.42	2636.57	2681.25	2681.25
f12	0.00	-28.32	31.46	31.46	0.00	-48.38	55.40	55.40
f22	1894.71	1830.83	2099.57	2042.21	1792.49	1747.62	1914.39	1914.39
f33	607.09	87.57	1883.48	658.96	481.89	120.09	1503.88	473.55
f44	607.09	87.57	658.96	1883.48	481.89	120.09	473.55	1503.88
λ			-1185.26				-1014.58	

Simulated Spectra

The above method was employed to simulate the photoelectron spectrum of C_2H^-, with the calculated transitions shown in Figure 3(a) alongside the experimental data at 355 nm. On the $\tilde{X}^2\Sigma^+$ surface, below 3,600 cm^{-1}, there is excellent agreement in both the transition positions and intensities between the simulated and experimental spectra. This includes the

HT coupled (2^{n+1}) transitions with Π symmetry, which would normally be missing from a simulation using standard *ab-initio* approaches.

The positions of the calculated levels for the $\tilde{A}^2\Pi$ state have been shifted by 1,220 cm^{-1} to account for the EOMIP-CCSDT calculations overestimating the effective Term energy. The experimental data shows that the electronic coupling interactions induce a splitting of the $\tilde{A}^2\Pi$ state origin over 5 vibronic levels, spaced by ~ 95 cm^{-1} $(a-e)$. This splitting is also observed in the calculated spectrum, which correctly predicts 5 prominent transitions in this region. The relative intensities between the calculated transitions are also in good agreement with the experimental data. Peak d is slightly underestimated, however the relative intensity difference between peaks d and e may be partly explained by the Wigner threshold law,[74] which will reduce the intensity of peak e in the experimental spectrum as it is close to the detachment threshold. The simulated spectrum also slightly underestimates the splitting between the vibronic levels, which may be linked to the overestimation of the gap between the $^2\Sigma$ and $^2\Pi$ surfaces.

The photoelectron spectrum of C_2D^- was also examined using the same approach, with the calculated transitions shown in Figure 3(b) alongside the 355 nm experimental data. Again, there is excellent agreement in the intensity and calculated positions of the transitions on the $\tilde{X}^2\Sigma^+$ state surface, including the HT coupled levels. Near the $\tilde{A}^2\Pi$ state origin, deuteration has a large impact on the experimental photoelectron spectrum. Instead of the 5 evenly split levels observed in C_2H, a single dominant peak (d) is now observed at 3,844 cm^{-1} alongside a collection of weaker peaks $(a-c)$ centred around 3,400 cm^{-1}. Based on previous spin-orbit splitting measurements, peak d is expected to have significant $\tilde{A}^2\Pi$ character, with peaks a-c commonly assigned to vibronic levels with predominantly HT coupled $\tilde{X}^2\Sigma^+$ character.[53,54,75,76] This suggests that deuteration effectively dampens the coupling interaction between the surfaces, as has been observed for HCCH.[77]

In agreement with the experimental spectra, a large change is observed in the simulated spectrum upon deuteration. The calculated intensity pattern of the vibronic levels around

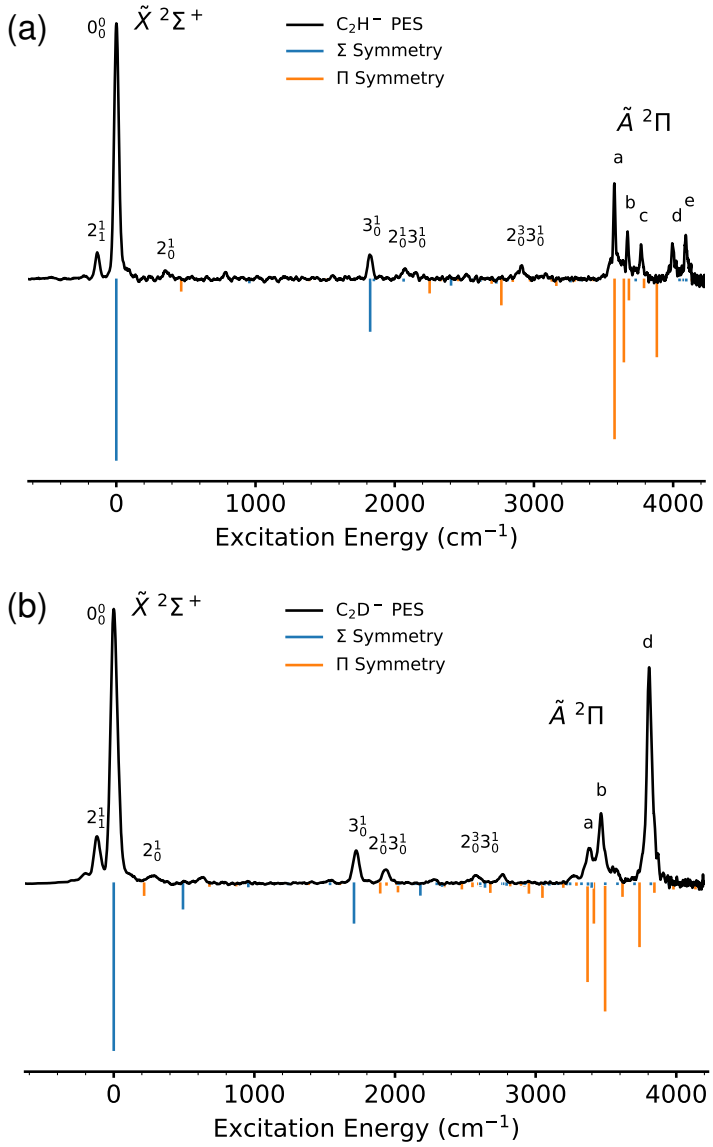

Figure 3: (a) Experimental photoelectron spectrum of C_2H^- at 355 nm, compared to the simulated spectrum calculated using the quasidiabatic ansatz. Transitions with Σ symmetry are shown in blue, transitions with Π symmetry are shown in orange. (b) Experimental photoelectron spectrum of C_2D^- at 355 nm, compared to the simulated spectrum. The labelling of peaks near the $\tilde{A}$ origin correspond to Table S1.

the $\tilde{A}^2\Pi$ origin is also a good match to the experimental data, with a single intense transition observed near peak d, and 3 prominent transitions predicted around the experimental peaks $a-c$. The calculated splitting between the levels is also similar, however the relative intensity of peak d appears to be slightly underestimated.

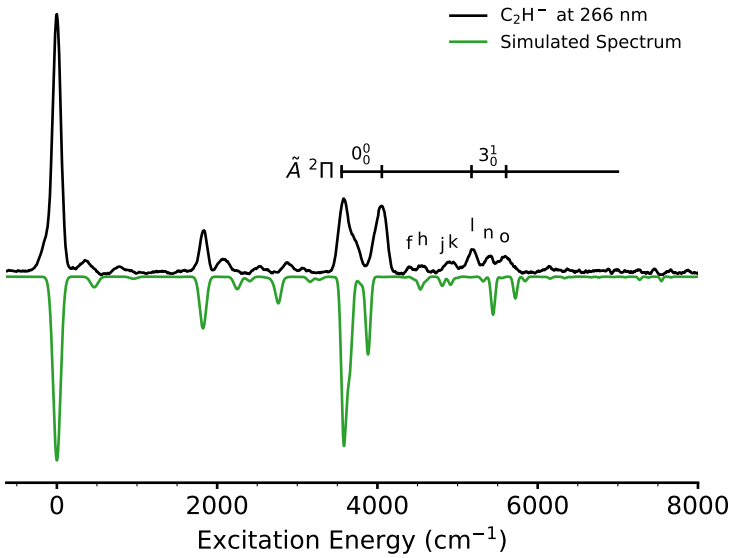

Figure 4: Photoelectron spectrum of C_2H^- at 266 nm, showing vibrationally excited $\tilde{A}$ state structure. The simulated spectra shown in green is calculated using the quasidiabatic ansatz, and convolved with Gaussians with a kinetic energy dependent FWHM of $\Delta E/E = 0.04\%$ ($\Gamma = 55 - 30$ cm^{-1}) to match the ~~lower~~ VMI resolution ~~at large electron kinetic energies~~ characteristics.

To investigate the effects of coupling on the higher excited vibronic levels on the $\tilde{A}^2\Pi$ surface, the calculations were also compared to the experimental photoelectron spectrum of C_2H^- at 266 nm, presented in Figure 4. Gaussians were fit to the transitions from Figure 3(a) with a FWHM of 40 cm^{-1} to match the lower resolution of the experimental data at high electron kinetic energies. Near 3,900 cm^{-1} the electronic origin of the $\tilde{A}^2\Pi$ state is split over 5 vibronic levels, as discussed above. A similar effect is also observed for the 3_0^1 band, which becomes split over 3 vibronic levels labelled l, n, and o. The calculated spectrum correctly predicts the position and intensity of peaks n and o, but appears to strongly underestimate the intensity of peak l. Between the 0_0^0 and 3_0^1 bands a collection of weaker peaks are also observed ($f - k$). These are assigned to highly excited HT coupled $\tilde{X}^2\Sigma^+$ transitions (j, k), admixed $\tilde{X} - \tilde{A}$ transitions (h, i) and pure $\tilde{X}^2\Sigma^+$ transitions (f). Consequently, peak f will possess Σ symmetry, and should have a different anisotropy to all of the other dominant transitions above 3,800 cm^{-1}. The position and intensity of these highly-excited coupled transitions are well described by the simulated spectrum.

The results from Figures 3 and 4 confirm that the quasiadiabtic approach is able to accurately describe the vibronic interactions between the $^2\Sigma^+$ and $^2\Pi$ surfaces, including deuteration effects. This validates the proposed vibronic interactions, and demonstrates how this method can be employed to decode and assign even complex spectra. Applying this approach to similar less-studied systems will produce reliable predictions for the position and intensity of dominant transitions, which will help guide the search for these molecules in laboratory experiments and astronomical observations.

Photoelectron Angular Distributions

Symmetry considerations may be employed to verify the spectral assignments from the calculations above. The quasidiabatic Hamiltonian approach is able to determine the symmetry of each individual vibronic state, either Σ or Π, which may be compared directly to the experimental electron anisotropy of each transition. The VMIs from this work (Figure 1) were obtained using a linearly polarized detachment laser. Therefore, the differential cross section of emitted electrons is given by

$$\frac{\mathrm{d}\sigma}{\mathrm{d}\Omega} = \frac{\sigma_{\mathrm{total}}}{4\pi}[1 + \beta P_2(\cos\theta)], \tag{10}$$

where θ is the angle between the ejected electron and the (vertical) laser polarization, and P_2 is the second-order Legendre polynomial. The anisotropy parameter β provides a quantitative measure of the anisotropy, and can range from -1 to +2, for purely perpendicular and parallel transition respectively. Through conservation of angular momentum, β may be described in terms of the detachment partial waves, which are linked to the symmetry of the parent detachment orbital. This is discussed in detail elsewhere,[78,79] and will be only briefly described for the case of C_2H^- here.

Photodetachment to the ground state of C_2H ($\tilde{X}\,^2\Sigma^+$) involves ejecting an electron from an $s-$like σ orbital (approximately $5\sigma_g$ in symmetry character), whereas detachment to

the excited $\tilde{A}\,^2\Pi$ state occurs from a $p-$like π orbital (approximately $1\pi_u$ in character).[64] Therefore, the electron anisotropies may be described using the mixed $s-p$ model,[78]

$$\beta_{sp}(\epsilon) = \frac{2(1-\gamma_p)B_1\epsilon + \gamma_p(2A_1^2\epsilon^2 - 4A_1\epsilon\cos\delta_{2,0})}{(1-\gamma_p)B_1\epsilon + \gamma_p(1+2A_1^2\epsilon^2)} \tag{11}$$

where ϵ is the electron kinetic energy and γ_p is the fraction of p character of the detachment orbital described as

$$|\psi\rangle = \sqrt{1-\gamma_p}|s\rangle + \sqrt{\gamma_p}|p\rangle. \tag{12}$$

A_1 and B_1 in Eq. (11) are the generalised Hanstorp[80] coefficients describing the assumed Wigner-like[74] relative scalings of the radial transition dipole matrix elements for different allowed detachment channels. Specifically, $A_1\epsilon$ describes the energy-dependent ratio of the $p \rightarrow d$ and $p \rightarrow s$ transition amplitudes, while $B_1\epsilon$ corresponds to the $s \rightarrow p$ and $p \rightarrow s$ cross-section ratio.[78] It can be shown that under certain approximations $B_1/A_1 = 8/3$.[81] Finally, $\delta_{2,0}$ in Eq. (11) is the phase shift between the s and d partial waves, which in most cases of anion photodetachment is assumed to be small, corresponding to $\cos\delta_{2,0} \approx 1$.

From Eq. (11) it can be seen that detachment from a pure s orbital ($\gamma_p = 0$) will have a positive anisotropy ($\beta = +2$), whereas detachment from a pure p orbital ($\gamma_p = 1$) will have a negative anisotropy for electron kinetic energies $\epsilon < 2/A_1$. Therefore, measuring the anisotropy can help determine the electronic character of each individual transition, which may be compared to the calculated symmetries in Figure 3. The anisotropy parameters were measured at a number of photon wavelengths every detachment wavelength for prominent transitions in the C_2H^- photoelectron spectra from this work, and are presented in Figure 5. Fitting Eq. (11) to the anisotropy parameters from $^2\Pi$ state detachment, with $\gamma_p = 0.9$ produces a Hanstorp coefficient of $A_1 = 0.66(4)$ eV^{-1}.

The sign (+/-) of β can be used to assign each vibronic level to either the $^2\Sigma^+ \leftarrow^1 \Sigma^+$ or $^2\Pi \leftarrow^1 \Sigma^+$ electronic transition respectively. This is particularly useful around the $\tilde{A}^2\Pi$ origin, where the two states mix overlap. It is important to note that the HT coupled transitions

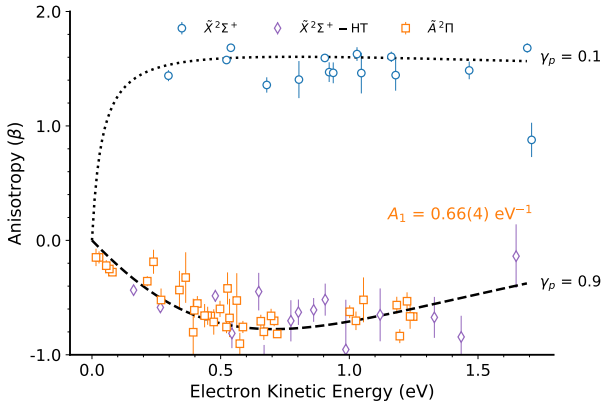

Figure 5: Photoelectron anisotropy parameters, measured for each resolved C_2H^- transition, across a range of detachment wavelengths. Allowed ground state transitions $\tilde{X}^2\Sigma^+$ are shown in orange, Herzberg-Teller coupled transitions are shown in purple, and excited state transitions $\tilde{A}^2\Pi$ are shown in blue. Anisotropy curves for a mixed-*sp* model (Eq. 11) are shown for $\gamma_p = 0.1$ and $\gamma_p = 0.9$.

on the $\tilde{X}^2\Sigma^+$ surface have negative anisotropies and Π symmetry. This is discussed in more detail in the Supplementary Materials.

represented as beta x I

A plot of the anisotropy parameters for C_2H^- detachment at 300 nm is presented in Figure 6, alongside the experimental spectrum. By plotting $\beta \times I$, allows the sign (+/-) of each individual transition ~~can~~ to be easily identified, even for partially resolved peaks. All of the transitions above the $\tilde{A}^2\Pi$ origin have a negative anisotropy, except for peak f. This confirms the assignment of this peak to the highly excited Σ transition $\tilde{X}(0,6,1)$, where $\tilde{X}(v_1,v_2,v_3)$. The nearby peaks h and i are assigned to the admixed Π transitions $\tilde{X}(0,3,2)\tilde{A}(0,0,0)$ and $\tilde{X}(0,7,1)\tilde{A}(010)$. The other two peaks in this region j and k are assigned to highly excited HT coupled Π transitions $\tilde{X}(0,7,1)$ and $\tilde{X}(0,11,0)$. The assignments for all peaks in the C_2H^- and C_2D^- photoelectron spectra are presented in the Supplementary Materials Table S1.

(Q: Are these Neumark's assignments, or yours from the synthetic model? This is not clear. Also, do they agree with Neumark?)

This result demonstrates how experimental anisotropies and calculated transition intensities can be used to help assign and understand vibronically coupled spectra. This is particularly useful in regions where there a large number of potential vibronic states, making definitive assignments based on energetics alone difficult.

(similar words, is there an alternative)

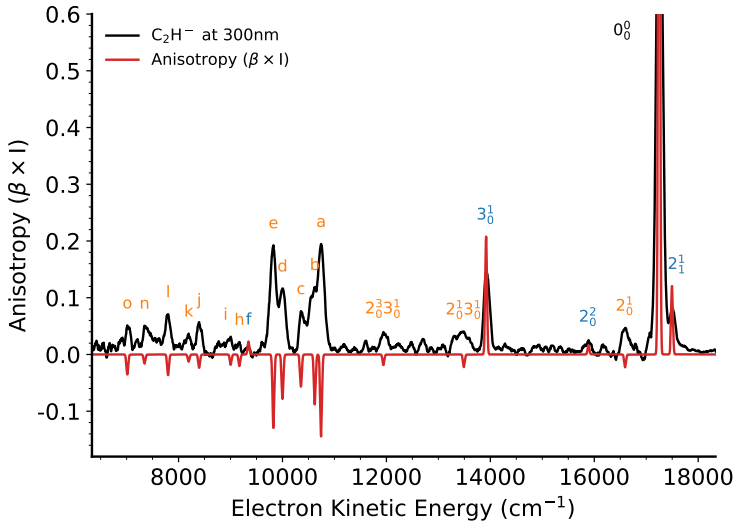

Figure 6: Photoelectron spectrum of C_2H^- at 300 nm, compared to anisotropy measurements ($\beta \times I$). For each resolved transition the anisotropy parameter was determined from Eq. (10) and multiplied by the corresponding photoelectron intensity. This allows for the sign (+/-) of each transitions to be readily determined.

Conclusions

High-resolution photoelectron images of C_2H^- and C_2D^- were recorded both at and above threshold, to investigate vibronic coupling effects in $C_{2n}H$ carbon monohydride chains. The interplay of pseudo Jahn-Teller and Renner Teller coupling between the close lying $\tilde{X}^2\Sigma^+$ and $\tilde{A}^2\Pi$ states results in a complex vibronic spectrum near the $\tilde{A}$ state surface, with the electronic origin split over multiple admixed levels.We have shown that by transforming to a quasidiabatic representation, the effect of these coupling interactions may be simulated. A KDC Hamiltonian was constructed, and parametrised using the CFOUR *ab-initio* computational package and the quasidiabatic ansatz. This resulted in simulated photoelectron spectra of C_2H^- and C_2D^- which closely resembled the experimental data, even near the complex $\tilde{A}$ state origin. Photoelectron anisotropy parameters were also calculated for each observed transitions across multiple wavelengths. Comparing the sign (+/-) of the anisotropy to the calculated vibronic symmetry allowed for even weak or partially resolved transitions to be assigned.

The excellent agreement between the experimental and calculated spectra in this work demonstrates that electronic spectra complicated by vibronic coupling effects may still be accurately simulated using outputs from standard *ab-initio* techniques, by transforming to a quasidiabatic representation. This approach may be extended to larger, less well known, $C_{2n}H$ chains, which may help guide the search for these molecules in astronomical studies, and help identify potential DIB carriers.

Methods

Details of the HR-PEI spectrometer are given in Refs 82 and 77. C_2H^- ions are produced by passing a 1:1 C_2H_4:O_2 gas mixture through a pulse valve, which then undergoes supersonic expansion into a high-voltage discharge. Negative ions are extracted, accelerated to 500 eV, and focussed into a novel gating, bunching, and re-referencing unit.[83] Anions are mass separated over a 2m time-of-flight region, with the ion of interest isolated by an electrostatic gate. The ion packet is crossed with a tuneable detachment laser beam, generated from a Continuum Sunlite EX optical parametric oscillator pumped by the third harmonic of a Continuum Powerlite 9010 Nd:YAG laser. The laser produces between 10-50mJ per pulse at 10Hz, depending on whether the idler or signal beam is used. The wavelength of the laser light is measured using a HighFinesse WS7 UV wavemeter.

A velocity-map imaging lens (modified version of the original concept of Eppink and Parker) images the detached electrons to a 75mm diameter MCP/phosphor screen detector. Events are imaged by a 2048x2048 monochrome CCD camera (PCO 2000), with each frame transferred to a computer at a 10Hz repetition rate, and processed in real time to identify individual electron events. The electron positions are centroided to a sub-pixel accuracy, then written to a data file for subsequent analysis. The velocity-map image is centred and then circularized by an angular dependent-radial scaling determined by comparing adjacent radial slice intensity profiles.[84] An inverse Abel transformation of the VMI, based on the algorithm

of Hansen and Law,[65,85] returns a slice image of the 3D electron source distribution. Absolute energy calibration of the photoelectron spectra is achieved using published measurements of species, including O^- [82] and NO_2^-,[79] that have been studied under similar conditions as used for the C_2H^- measurements.

In standard operation, the energy distribution of the detached electrons is obtained by recording the velocity-mapped positions from photodetachment at a fixed wavelength. However the HR-PEI spectrometer may also be reconfigured into an electron counting mode, where the number of events per laser shot is recorded, while the detachment laser wavelength is varied.

(True, but this aspect is not used in this work)

Acknowledgement

This research was supported by the Australian Research Council Discovery Project Grants DP160102585 and DP190103151.

References

(Is there a published paper, rather than a conference paper = why is this work particularly important?)

(1) Frenklach, M.; Clary, D. W.; Gardiner, W. C.; Stein, S. E. Detailed kinetic modeling of soot formation in shock-tube pyrolysis of acetylene. *Symposium (International) on Combustion* **1985**, *20*, 887 – 901, Twentieth Symposium (International) on Combustion.

(2) Boullart, W.; Devriendt, K.; Borms, R.; Peeters, J. Identification of the Sequence $CH(^2\Pi) + C_2H_2 \rightarrow C_3H_2 + H$ (and $C_3H + H_2$) Followed by $C_3H_2 + O \rightarrow C_2H + HCO$ (or H + CO) as C_2H Source in C_2H_2/O/H Atomic Flames. *The Journal of Physical Chemistry* **1996**, *100*, 998–1007.

(3) Irvine, W. M.; Ohishi, M.; Kaifu, N. Chemical abundances in cold, dark interstellar clouds. *Icarus* **1991**, *91*, 2–6.

(4) Vuitton, V.; Scemama, A.; Gazeau, M.-C.; Chaquin, P.; BÃľnilan, Y. IR and UV spectroscopic data for polyynes: Predictions for long carbon chain compounds in Titan's atmosphere. *Advances in Space Research* **2001**, *27*, 283–288.

(5) Wilson, E.; Atreya, S. Chemical sources of haze formation in Titan's atmosphere. *Planetary and Space Science* **2003**, *51*, 1017–1033, Surfaces and Atmospheres of the Outer Planets their Satellites and Ring Systems.

(6) Dobrijevic, M.; Loison, J.; Hickson, K.; Gronoff, G. 1D-coupled photochemical model of neutrals, cations and anions in the atmosphere of Titan. *Icarus* **2016**, *268*, 313 – 339.

(7) Jackson, W. M.; Blunt, V.; Lin, H.; Green, M.; Olivera, G.; Fink, W. H.; Bao, Y.; Urdahl, R. S.; Mohammad, F.; Zahedi, M. Non-adiabatic interactions in excited C_2H molecules and their relationship to C_2 formation in comets. *Astrophysics and Space Science* **1996**, *236*, 29–47.

(8) Ziurys, L. M.; Saykally, R. J.; Plambeck, R. L.; Erickson, N. R. Detection of the N=3-2 transition of CCH in Orion and determination of the molecular rotational constants. *The Astrophysical Journal* **1982**, *254*, 94–99.

(9) Gupta, H.; Gottlieb, C. A.; McCarthy, M. C.; Thaddeus, P. A Survey of C_4H, C_6H, and C_6H^- with the Green Bank Telescope. *The Astrophysical Journal* **2009**, *691*, 1494–1500.

(10) Beuther, H.; Semenov, D.; Henning, T.; Linz, H. Ethynyl (C_2H) in Massive Star formation: Tracing the Initial Conditions? *The Astrophysical Journal Letters* **2008**, *675*, L33.

(11) Jiang, X.-J.; Liu, H. B.; Zhang, Q.; Wang, J.; Zhang, Z.-Y.; Li, J.; Gao, Y.; Gu, Q. SMA Observations of C_2H in High-Mass Star-Forming Regions. *The Astrophysical Journal* **2015**, *808*, 114.

(12) Douglas, A. Origin of diffuse interstellar lines. *Nature* **1977**, *269*, 130–132.

(13) Fulara, J.; Lessen, D.; Freivogel, P.; Maier, P. Laboratory evidence for highly unsaturated hydrocarbons as carriers of some of the diffuse interstellar bands. *Nature* **1993**, *366*, 439–441.

(14) Watson, J. K. Homologous Series of Diffuse Interstellar Bands. *The Astrophysical Journal* **1994**, *437*, 678.

(15) Fulara, J.; KreÅĆowski, J. Origin of diffuse interstellar bands: spectroscopic studies of their possible carriers. *New Astronomy Reviews* **2000**, *44*, 581–597.

(16) Schmidt Timothy W., S. R. G. The Optical Spectroscopy of Extraterrestrial Molecules. *Australian Journal of Chemistry* **2005**, *58*, 69–81.

(17) Millar, T. J.; Walsh, C.; Field, T. A. Negative Ions in Space. *Chemical Reviews* **2017**, *117*, 1765–1795, PMID: 28112897.

(18) McCarthy, M. C.; Gottlieb, C. A.; Gupta, H.; Thaddeus, P. Laboratory and Astronomical Identification of the Negative Molecular Ion C_6H^-. *The Astrophysical Journal* **2006**, *652*, L141–L144.

(19) Cernicharo, J.; Guélin, M.; Agúndez, M.; Kawaguchi, K.; McCarthy, M.; Thaddeus, P., Astronomical detection of C_4H^-, the second interstellar anion*. *A&A* **2007**, *467*, L37–L40.

(20) BrÃijnken, S.; Gupta, H.; Gottlieb, C. A.; McCarthy, M. C.; Thaddeus, P. Detection of the Carbon Chain Negative Ion C_8H^- in TMC-1. *The Astrophysical Journal* **2007**, *664*, L43–L46.

(21) Remijan, A. J.; Hollis, J. M.; Lovas, F. J.; Cordiner, M. A.; Millar, T. J.; Markwick-Kemper, A. J.; Jewell, P. R. Detection of C_8H^- and Comparison with C_8H toward IRC +10 216. *The Astrophysical Journal* **2007**, *664*, L47–L50.

(22) Cordiner, M. A.; Buckle, J. V.; WirstrÃűm, E. S.; Olofsson, A. O. H.; Charnley, S. B. On the Ubiquity of Molecular Anions in the Dense Interstellar Medium. *The Astrophysical Journal* **2013**, *770*, 48.

(23) Sakai, N.; Shiino, T.; Hirota, T.; Sakai, T.; Yamamoto, S. Long Carbon-Chain Molecules and their Anions in the Starless Core LUPUS-1A. *The Astrophysical Journal* **2010**, *718*, L49–L52.

(24) Sakai, N.; Sakai, T.; Yamamoto, S. Tentative Detection of C_4H^- toward the Low-Mass Protostar IRAS 04368+2557 in L1527. *The Astrophysical Journal* **2007**, *673*, L71–L74.

(25) Herbst, E.; Osamura, Y. Calculations on the Formation Rates and Mechanisms for CnH Anions in Interstellar and Circumstellar Media. *The Astrophysical Journal* **2008**, *679*, 1670–1679.

(26) Bastian, B.; Michaelsen, T.; Meyer, J.; Wester, R. Anionic Carbon Chain Growth in Reactions of C_2^-, C_4^-, C_6^-, C_2H^-, C_4H^-, and C_6H^- with C_2H_2. *The Astrophysical Journal* **2019**, *878*, 162.

(27) Vuitton, V.; Lavvas, P.; Yelle, R.; Galand, M.; Wellbrock, A.; Lewis, G.; Coates, A.; Wahlund, J.-E. Negative ion chemistry in Titan's upper atmosphere. *Planetary and Space Science* **2009**, *57*, 1558–1572, Surfaces and Atmospheres of the Outer Planets, Their Satellites and Ring Systems: Part V.

(28) Desai, R. T.; Coates, A. J.; Wellbrock, A.; Vuitton, V.; Crary, F. J.; González-Caniulef, D.; Shebanits, O.; Jones, G. H.; Lewis, G. R.; Waite, J. H. et al. Carbon Chain Anions and the Growth of Complex Organic Molecules in Titan's Ionosphere. *The Astrophysical Journal* **2017**, *844*, L18.

(29) Mukundan, V.; Bhardwaj, A. A Model for Negative Ion Chemistry in Titan's Ionosphere. *The Astrophysical Journal* **2018**, *856*, 168.

(30) Maier, J. P. Electronic spectroscopy of carbon chains. *Chemical Society Reviews* **1997**, *26*, 21–28.

(31) Fortenberry, R. C.; King, R. A.; Stanton, J. F.; Crawford, T. D. A benchmark study of the vertical electronic spectra of the linear chain radicals C_2H and C4H. *The Journal of Chemical Physics* **2010**, *132*, 144303.

(32) Curl, R. F.; Carrick, P. G.; Merer, A. J. Rotational analysis of the $\tilde{A} \leftarrow \tilde{X}$ system of C_2H. *The Journal of Chemical Physics* **1985**, *82*, 3479–3486.

(33) Tarroni, R.; Carter, S. Theoretical calculation of vibronic levels of C_2H and C_2D to 10,000 cm^{-1}. *The Journal of Chemical Physics* **2003**, *119*, 12878–12889.

(34) Zhou, J.; Garand, E.; Neumark, D. M. Slow electron velocity-map imaging spectroscopy of the C_4H^- and C_4D^- anions. *The Journal of Chemical Physics* **2007**, *127*, 154320.

(35) Linnartz, H.; Motylewski, T.; Vaizert, O.; Maier, J.; Apponi, A.; McCarthy, M.; Gottlieb, C.; Thaddeus, P. Electronic Ground and Excited State Spectroscopy of C6H and C6D. *Journal of Molecular Spectroscopy* **1999**, *197*, 1–11.

(36) Taylor, T. R.; Xu, C.; Neumark, D. M. Photoelectron spectra of the $C_{2n}H^-$ (n=1-4) and $C_{2n}D^-$ (n=1-3) anions. *The Journal of Chemical Physics* **1998**, *108*, 10018–10026.

(37) Matthews, D. A.; Cheng, L.; Harding, M. E.; Lipparini, F.; Stopkowicz, S.; Jagau, T.-C.; Szalay, P. G.; Gauss, J.; Stanton, J. F. Coupled-cluster techniques for computational chemistry: The CFOUR program package. *The Journal of Chemical Physics* **2020**, *152*, 214108.

(38) Heikkilä, A.; Johansson, L. E. B.; Olofsson, H. Molecular abundance variations in the Magellanic Clouds. *Astronomy & Astrophysics* **1999**, *344*, 817–847.

(39) Cochran, E. L.; Adrian, F. J.; Bowers, V. A. ESR Study of Ethynyl and Vinyl Free Radicals. *The Journal of Chemical Physics* **1964**, *40*, 213–220.

(40) Jinguji, M.; McDowell, C.; Shimokoshi, K. High-resolution ESR spectrum of the ethynyl radical in an argon matrix at 4.2 K. *Journal of Molecular Structure* **1985**, *130*, 317–326.

(41) Brown, J. M.; Evenson, K. M. The far-infrared laser magnetic resonance spectrum of vibrationally excited C_2H. *Journal of Molecular Spectroscopy* **1988**, *131*, 161–171.

(42) Pfelzer, C.; Havenith, M.; PeriÄĞ, M.; MÃijrtz, P.; Urban, W. Faraday Laser Magnetic Resonance Spectroscopy of Vibrationally Excited C_2H. *Journal of Molecular Spectroscopy* **1996**, *176*, 28–37.

(43) Schmidt, C.; PeriÄĞ, M.; MÃijrtz, P.; Wienkoop, M.; Havenith, M.; Urban, W. Faraday Laser Magnetic Resonance Spectroscopy of Vibrationally Excited C_2D. *Journal of Molecular Spectroscopy* **1998**, *190*, 112–124.

(44) Sastry, K. V. L. N.; Helminger, P.; Charo, A.; Herbst, E.; De Lucia, F. C. Laboratory millimeter and submillimeter spectrum of CCH. *The Astrophysical Journal* **1981**, *251*, L119.

(45) Gottlieb, C. A.; Gottlieb, E. W.; Thaddeus, P. Laboratory and astronomical measurement of the millimeter wave spectrum of the ethynyl radical CCH. *The Astrophysical Journal* **1983**, *264*, 740–745.

(46) Endo, Y.; Kanamori, H.; Hirota, E. Millimeter- and submillimeter-wave spectra of the vibrationally excited CCD radical. *Chemical Physics Letters* **1989**, *160*, 280–284.

(47) Müller, H. S. P.; Klaus, T.; Winnewisser, G. Submillimeter-wave spectrum of the ethynyl radical, CCH, up to 1 THz. *Astronomy and Astrophysics* **2000**, *357*, L65–L67.

(48) Shepherd, R. A.; Graham, W. R. M. FTIR study of D and 13C substituted C_2H in solid argon. *The Journal of Chemical Physics* **1987**, *86*, 2600–2605.

(49) Jacox, M. E.; Olson, W. B. The $\tilde{A}^2\Pi - \tilde{X}^2\Sigma^+$ transition of HC_2 isolated in solid argon. *The Journal of Chemical Physics* **1987**, *86*, 3134–3142.

(50) Forney, D.; Jacox, M.; Thompson, W. The Infrared and Near-Infrared Spectra of HCC and DCC Trapped in Solid Neon. *Journal of Molecular Spectroscopy* **1995**, *170*, 178–214.

(51) Vervloet, M.; Herman, M. Fourier transform emission spectroscopy of C_2H. *Chemical Physics Letters* **1988**, *144*, 48–50.

(52) Hsu, Y.; Lin, J. J.; PapouÅąek, D.; Tsai, J. The lowâĂŘlying bending vibrational levels of the CCH ($\tilde{X}^2\Sigma^+$) radical studied by laserâĂŘinduced fluorescence. *The Journal of Chemical Physics* **1993**, *98*, 6690–6696.

(53) Hsu, Y.; Shiu, Y.; Lin, C. LaserâĂŘinduced fluorescence spectroscopy of CCH ($\tilde{X}^2\Sigma^+$) in vibrationally excited levels up to 4500 cm^{-1}. *The Journal of Chemical Physics* **1995**, *103*, 5919–5930.

(54) Chiang, W.-Y.; Hsu, Y.-C. Laser spectroscopy of CCH in the 36,600-39,700 cm^{-1} region. *The Journal of Chemical Physics* **1999**, *111*, 1454–1461.

(55) Ervin, K. M.; Lineberger, W. C. Photoelectron spectra of dicarbon(1-) and ethynyl(1-). *The Journal of Physical Chemistry* **1991**, *95*, 1167–1177.

(56) PeriÄĞ, M.; Peyerimhoff, S. D.; Buenker, R. J. Ab initio investigation of the vibronic structure of the C_2H spectrum. *Molecular Physics* **1990**, *71*, 693–719.

(57) PeriÄĞ, M.; Reuter, W.; Peyerimhoff, S. D. Ab initio investigation of the vibronic structure in the C_2H spectrum: Spin-orbit splitting of the vibronic levels. *Journal of Molecular Spectroscopy* **1991**, *148*, 201–212.

(58) PeriÄĞ, M.; Peyerimhoff, S. D.; Buenker, R. J. Ab initio investigation of the vibronic structure in the C_2H spectrum: Calculation of vibronic energies and wavefunctions for various isotopomers. *Journal of Molecular Spectroscopy* **1991**, *148*, 180–200.

(59) PeriÄĞ, M.; Engels, B.; Peyerimhoff, S. D. Ab initio investigation of the vibronic structure of the C_2H spectrum: Computation of the vibronically averaged values for the hyperfine coupling constants. *Journal of Molecular Spectroscopy* **1991**, *150*, 70–85.

(60) PeriÄĞ, M.; Peyerimhoff, S.; Buenker, R. Analysis and predictions of the vibronic spectrum of the ethynyl radical C_2H by ab initio methods. *Z Phys D - Atoms, Molecules and Clusters* **1992**, *24*, 177–198.

(61) Carter, S.; Handy, N. C.; Puzzarini, C.; Tarroni, R.; Palmieri, P. A variational method for the calculation of spin-rovibronic energy levels of triatomic molecules with three interacting electronic states. *Molecular Physics* **2000**, *98*, 1697–1712.

(62) Tarroni, R.; Carter, S. Theoretical calculation of absorption intensities of C_2H and C_2D. *Molecular Physics* **2004**, *102*, 2167–2179.

(63) Stanton, J. F. Why the CC Stretch in HCC Is So Anharmonic. *The Journal of Physical Chemistry A* **2021**, *125*, 7694–7698.

(64) Gulania, S.; Krylov, A. I. Dissociative electron attachment in C_2H via electronic resonances. *Molecular Physics* **2021**, *119*, e1979262.

(65) Hickstein, D. D.; Gibson, S. T.; Yurchak, R.; Das, D. D.; Ryazanov, M. A direct comparison of high-speed methods for the numerical Abel transform. *Review of Scientific Instruments* **2019**, *90*, 065115.

(66) Köuppel, H.; Domcke, W.; Cederbaum, L. S. *Advances in Chemical Physics*; John Wiley & Sons, Ltd, 1984; pp 59–246.

(67) Domcke, W.; KÃűppel, H.; Cederbaum, L. Spectroscopic effects of conical intersections of molecular potential energy surfaces. *Molecular Physics* **1981**, *43*, 851–875.

(68) Pacher, T.; Cederbaum, L. S.; KÃűppel, H. *Advances in Chemical Physics*; John Wiley & Sons, Ltd, 1993; pp 293–391.

(69) Stanton, J. F. Quantitative vibronic coupling calculations. The visible spectrum of propadienylidene. *Faraday Discuss.* **2011**, *150*, 331–343.

(70) Ichino, T.; Gianola, A. J.; Lineberger, W. C.; Stanton, J. F. Nonadiabatic effects in the photoelectron spectrum of the pyrazolide-d3 anion: Three-state interactions in the pyrazolyl-d3 radical. *The Journal of Chemical Physics* **2006**, *125*, 084312.

(71) Ichino, T.; Wren, S. W.; Vogelhuber, K. M.; Gianola, A. J.; Lineberger, W. C.; Stanton, J. F. The vibronic level structure of the cyclopentadienyl radical. *The Journal of Chemical Physics* **2008**, *129*, 084310.

(72) Ichino, T.; Gauss, J.; Stanton, J. F. Quasidiabatic states described by coupled-cluster theory. *The Journal of Chemical Physics* **2009**, *130*, 174105.

(73) Weichman, M. L.; Cheng, L.; Kim, J. B.; Stanton, J. F.; Neumark, D. M. Low-lying vibronic level structure of the ground state of the methoxy radical: Slow electron velocity-map imaging (SEVI) spectra and KÃűppel-Domcke-Cederbaum (KDC) vibronic Hamiltonian calculations. *The Journal of Chemical Physics* **2017**, *146*, 224309.

(74) Wigner, E. P. On the Behavior of Cross Sections Near Thresholds. *Physical Review* **1948**, *73*, 1002–1009.

(75) Yan, W.-B.; Dane, C.; Zeitz, D.; Hall, J. L.; Curl, R. Color center laser spectroscopy of C_2H and C_2D. *Journal of Molecular Spectroscopy* **1987**, *123*, 486–495.

(76) Sharp-Williams, E. N.; Roberts, M. A.; Nesbitt, D. J. Dark state vibronic coupling in the $\tilde{A}^2\Pi \leftarrow \tilde{X}^2\Sigma^+$ band of ethynyl radical via high resolution infrared absorption spectroscopy. *Physical Chemistry Chemical Physics* **2011**, *13*, 17474–17483.

(77) DeVine, J. A.; Weichman, M. L.; Laws, B.; Chang, J.; Babin, M. C.; Balerdi, G.; Xie, C.; Malbon, C. L.; Lineberger, W. C.; Yarkony, D. R. et al. Encoding of vinylidene isomerization in its anion photoelectron spectrum. *Science* **2017**, *358*, 336–339.

(78) Khuseynov, D.; Blackstone, C. C.; Culberson, L. M.; Sanov, A. Photoelectron angular distributions for states of any mixed character: An experiment-friendly model for atomic, molecular, and cluster anions. *The Journal of Chemical Physics* **2014**, *141*, 124312.

(79) Laws, B. A.; Cavanagh, S. J.; Lewis, B. R.; Gibson, S. T. Wigner Near-Threshold Effects in the Photoelectron Angular Distribution of NO2âĂŞ. *The Journal of Physical Chemistry A* **2019**, *123*, 10418–10425.

(80) Hanstorp, D.; Bengtsson, C.; Larson, D. J. Angular distributions in photodetachment from O^-. *Physical Review A* **1989**, *40*, 670–675.

(81) Sanov, A.; Grumbling, E. R.; Goebbert, D. J.; Culberson, L. M. Photodetachment anisotropy for mixed s-p states: 8/3 and other fractions. *The Journal of Chemical Physics* **2013**, *138*, 054311.

(82) Cavanagh, S. J.; Gibson, S. T.; Gale, M. N.; Dedman, C. J.; Roberts, E. H.; Lewis, B. R. High resolution velocity-map imaging photoelectron spectroscopy of the O^- fine-structure transitions. *Physical Review A* **2007**, *76*, 052708.

(83) Dedman, C. J.; Roberts, E. H.; Gibson, S. T.; Lewis, B. R. Fast 1 kV metal-oxide-semiconductor field-effect transistor switch. *Review of Scientific Instruments* **2001**, *72*, 3718–3720.

(84) Gascooke, J. R.; Gibson, S. T.; Lawrance, W. D. AˆâĂIJcircularisationâĂİ method to repair deformations and determine the centre of velocity map images. *The Journal of Chemical Physics* **2017**, *147*, 013924.

(85) Hansen, E. W.; Law, P.-L. Recursive methods for computing the Abel transform and its inverse. *Journal of the Optical Society of America A* **1985**, *2*, 510–520.